Landau theory for stress-induced, order-disorder transitions in phase change materials

Matthias Thielen,[1] Razvan A. Nistor,[2] Dmitryi Shakhvorostov,[1]
Guillermo Beltramo,[3] Margret Giesen,[3] and Martin H. Müser[1,4,*]

[1]*Dept. of Materials Science and Engineering, Universität des Saarlandes, Saarbrücken, Germany*
[2]*Dept. of Chemistry, Columbia University, New York, NY 10027*
[3]*Institute of Complex Systems ICS-7, FZ Jülich, Jülich, Germany*
[4]*Jülich Supercomputing Centre, Institute for Advanced Simulation, FZ Jülich, Jülich, Germany*

We propose a Landau theory for phase change materials (PCMs), which describes stress-induced amorphization in vacancy-free, ordered PCMs as a condensation of defects in analogy to equilibrium gas-liquid transitions. Three dimensionless parameters suffice to deduce a highly-accurate equation of state for both phases from it. The reference data for our model alloy Ge_xSb_{1-x} is produced from molecular dynamics simulations and synchrotron X-ray diffraction (XRD). Raman spectroscopy is used to estimate the density of tetrahedrally coordinated germanium atoms, which we relate to the order parameter. All methods provide consistent support for the reversibility of the transition.

PACS numbers: 61.43.Dq, 61.43.Bn, 61.46.-w

I. INTRODUCTION

Optoelectronic phase change materials (PCM) have markedly different optical reflectivity and electrical conductivity in their disordered and ordered phases.[1] They can be switched rapidly and reversibly between their better conducting crystalline and the more insulating amorphous phases. Short intense and long low-intensity heat or laser pulses induce the amorphous and the crystalline phase respectively.[2–4] Owing to their properties, PCMs are used as non-volatile memory materials and bear promise as materials for programmable logic circuits.[5]

Recently, the response of PCMs to pressure has received increased attention, mainly for the commercially used $Ge_2Sb_2Te_5$[6–10] but also for Ge_xSb_{1-x}.[11,12] These studies were motivated predominantly by the desire to unravel the interplay between atomic and electronic structure. Understanding PCMs under pressure might prove especially useful in the debate if the peculiar properties of PCMs arise either due to a difference of local order between crystalline and disordered phases, or because the absence of long-range order in the glass suppresses resonance bonding.[13]

In the mentioned PCMs and related compounds, the crystalline structures can be derived from simple cubic crystals by introducing a Peierls deformation and/or by (partially[14]) ordering the Ge, Sb, and Te atoms, as well as vacancies, onto sublattices. In these structures, the coordination shell of atoms can be described as ideal, distorted, or defective octahedra. According to various groups, the local arrangement of atoms can differ in the glass:[11,15–22] a significant fraction of germanium atoms have four short bonds with predominantly tetrahedral coordination.

The application of pressure allows one to alter local coordination without changing composition or temperature. This in turn can elucidate the relaxation dynamics in the glass. For example, one could use pressure to squeeze some germanium atoms from a small, e.g., tetrahedral shell (possible in the glass) into a larger, octahedral shell (only allowed coordination in the crystal). Once the pressure is released, one can determine if they remain at their new positions or if they move back to a "glass-like" coordination. If the latter happens, a well-defined number of germanium atoms with local glassy coordination might exist, which could make it possible to describe the disordered phase with an equilibrium theory.

Support for the idea that local order plays the predominant role in some disordered PCMs can be deduced from density functional theory (DFT) based molecular dynamics simulations:[23] after sudden changes in either volume or temperature, the stress in glassy PCMs quickly approached that observed experimentally — already after times too short for atoms to move much more than one or two Angstroms. Moreover the relaxation occurred such that several parameters, including the mean coordination number of Ge atoms, moved *away* from the crystalline reference values as the glass aged. This is consistent with the later observation[24] that the resistivity of the glassy $Ge_{15}Sb_{85}$ slowly increases with time rather than to approach the conducting, crystalline state. This could imply that a well-defined meta-stable glassy state exists, whose vicinity is approached rather quickly even if long-time relaxation may be necessary to fully reach it.

In this work, we explore possibilities to construct a Landau theory for PCMs. Since, the transition between crystal and glass can be invoked by stress without passing an intermediate liquid phase,[9–11] we use pressure rather than temperature as the driving force. The equation of state (EOS) that is deduced from the theory is compared to new experimental and numerical data. To isolate the effect of local coordination from that of the squeeze-out of vacancies, we restrict our attention to PCMs with a negligible number of vacancies in the crystal. We thus disregard any GeTe-Sb_2Te_3 pseudo binary alloys, also because these alloys lie close to the flexible part of a Maxwell-rigidity contour map[22], where glassy relaxation is non-negligible.

An additional incentive to focus on Ge_xSb_{1-x} is that stress-induced amorphization and crystallization in these alloys occur at more moderate pressures than in $Ge_2Sb_2Te_5$, i.e., at estimated pressures of $p_a = -4$ GPa for $x = 0.15$ (tensile pressure for amorphization) and $p_c = 2$ GPa (crystallization) versus $p_{a,c} = \mathcal{O}(20$ GPa). Moreover, a Maxwell rigidity analysis of Ge_1Sb_6 indicated that this alloy has a large number of constraints implying a large connectedness reducing second-neighbor motion[22], whereby relaxation in the glass should be small. Lastly, the transitions in our alloys occur between the technologically relevant phases, which are both (meta–) stable at ambient conditions. Thus, if the transition turns out reversible, it could become possible to switch our alloys through small-scale piezoelectric actuators. If the technical challenges could be solved,[5] stress switching should be faster and less energy demanding than thermal switching, which excites many "irrelevant" modes and is furthermore limited by thermal conductivity rather than by the speed of sound.

II. METHODS

A. Experimental methods

The Landau theory presented in this work is compared to experimental and numerical results on Ge_xSb_{1-x}. In our experiments, we used the same diamond anvil cell (DAC) and followed the same protocol as that described in Ref. 12, except that this time, additional experiments were conducted at the PDIFF Beamline (at 19.0 keV; $\lambda = 0.06525$ nm) of the ANKA synchrotron at the KIT. Densities of the amorphous phase were deduced from the broad peaks, which were gauged by using the well known 8% density difference for the amorphous and crystalline phase, which coincided with the density difference seen in our simulations. We refer the reader to Refs. 11 and 24 to justify the comparison between the sputtered experimental samples and temperature- or pressure-quenched in silico samples.

XRD spectra, representative of those from which we deduced equations of state, are shown in Fig. 1. The load and relieve cycle begins at the bottom and ends at the top. Broad peaks at ambient pressure are indicative of the amorphous state. With increasing pressure, a phase transformation occurs. Coexistence of both phases is observed at 1.7 GPa, where sharp but low-intensity Bragg peaks can be seen in addition to the broad features. After crystallization a Peierls distorted structure emerges. As observed previously, the distortion is reduced with increasing pressure, as evidenced by the convergence of the (104) and (110) peaks. At 12.8 GPa the Peierls distortion is entirely squeezed out and a simple cubic structure results. After decompression, the Peierls distorted structure is restored and the peaks are separated again. A transformation back to the amorphous state from high pressures does not occur in this example.

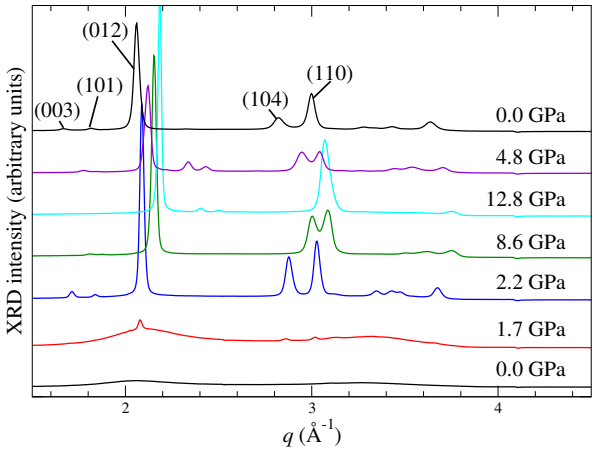

FIG. 1: (Color online) Representative X-ray spectra of $Ge_{0.15}Sb_{0.85}$ during compression and subsequent decompression. The bottom spectrum represents the initial sample.

Raman spectroscopy was performed using a WiTec alpha 300R Raman system with 532 nm excitation emerging from a frequency-doubled Nd:YAG laser. The power density at the sample was kept at a low level to avoid crystallization, while the spectra were detected by a cooled CCD. The power density at the sample was kept at a low level to avoid crystallization. The laser power was 0.3 mW at a focus spot of ~ 7 μm diameter with a Mitutoyo M Plan Apo 20x (long working distance) objective. The pressure was determined in the ruby fluorescence method[25].

In more detail, Raman images (50×50 pixels, 80×80 μm^2) were recorded using a 1800 grid. Each pixel contained a full Raman spectrum between approximately 0 and 1200 cm^{-1}. The raw Raman spectra in each pixel represent a set of potential mixtures of different chemical stoicheometries or structural phases — depending on the displayed sample position. The Raman spectra are represented by a matrix $\mathbf{M}$, where spectral intensities are given by the matrix rows and spectral frequencies are found in the matrix columns. For a Raman scan of N pixels with K frequencies, $\mathbf{M}$ is a $N \times K$ matrix. The Raman scans, respectively the intensity matrix were analyzed using Principal Component Analysis (PCA)[26,27], a mathematical procedure based on orthogonal transformations to convert (experimental, possibly linearly dependent) observations into linear independent (orthogonal) observations, the principal components (PC). PCA is frequently used to analyze spectroscopy data[28–34]. The PCs are sorted with respect to descending variance along their principal axes. The PCA expresses the matrix $\mathbf{M}$ as the product of two new matrices $\mathbf{S}$ (scores) and $\mathbf{L}$ (loadings), $\mathbf{M} = \mathbf{S}\mathbf{L}^T$. The scores are the coordinates of the original raw spectra in the new coordinate system of the principal components. Raman spectra of different chemical components or different phases are then generally recovered as different principal components.

We used the standard algorithms for PCA analysis as

implemented in the Matlab statistics toolbox (version 7.11.0 R2010b, Mathworks Inc.). The raw data was preprocessed using a Matlab based cosmic ray removal filter. Additional preprocessing, such as for instance background subtraction was not necessary and therefore not applied. A homogeneous background signal is automatically accounted for in the PCA.

Fig. 2 shows representative Raman spectra of initially amorphous $Ge_{0.15}Sb_{0.85}$ obtained from the PCA analysis. At 1.5 GPa, first signs of the crystalline phase can be observed. The transition appears nearly complete at 2.0 GPa. Further compression is followed by peak shiftings due to mode stiffening.

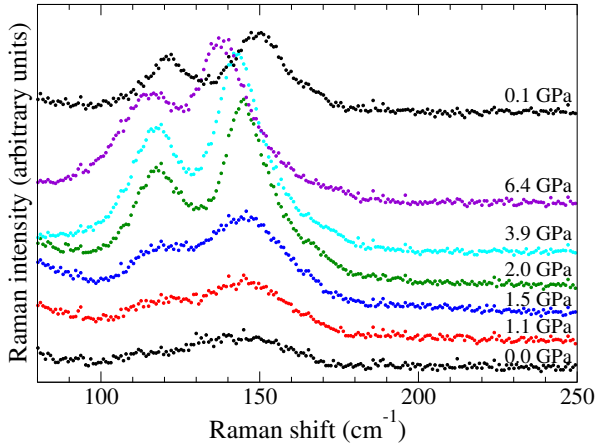

FIG. 2: (Color online) Typical Raman spectra of $Ge_{0.15}Sb_{0.85}$ at different pressures. The bottom spectrum represents the initial sample.

To obtain information about the microscopic order, Raman spectra were fitted to a superposition of Gaussians. Representative fits are shown in Fig. 3 for spectra obtained from (a) an amorphous and (b) a crystalline $Ge_{0.15}Sb_{0.85}$ alloy. Differences are revealed in white-light images of the sample inside the DAC, as evidenced in Fig. 4.

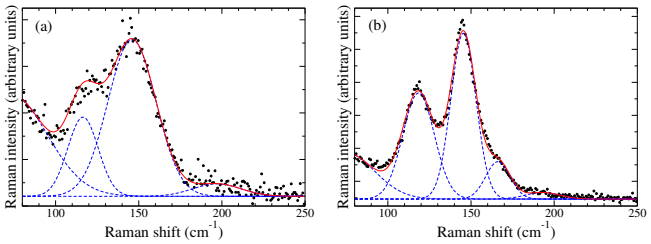

FIG. 3: (Color online) Raman spectra of (a) an amorphous sample at 1.0 GPa and (b) a crystalline sample at 2.0 GPa. Dashed blue lines are individual Gaussians fitted to the spectra. Solid red lines represent the sum of the blue lines.

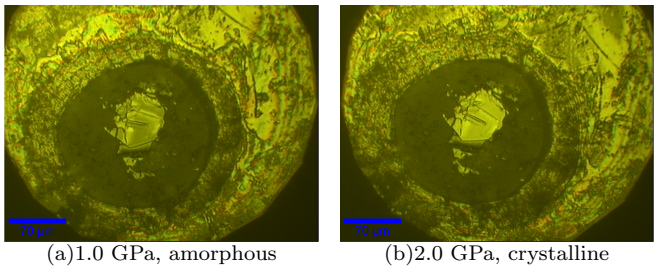

(a)1.0 GPa, amorphous (b)2.0 GPa, crystalline

FIG. 4: (Color online) Optical images of the sample giving rise to the spectra shown in Fig. 3.

B. Numerical methods

For the simulations, we used the same DFT-based MD method as in Ref. 11 and Chapter 5 in Ref. 35. The system was composed 28 Ge and 164 Sb atoms. The nuclear and electronic degrees of freedom were propagated within the Car-Parrinello molecular dynamics (CPMD) framework[36] using a plane-wave basis with an energy cutoff of 35 Ryd and the B-LYP density functional to approximate electronic exchange and correlation effects.[37,38] Nosé-Hoover chain thermostats[39] were used to ensure constant temperature and adiabatic separation of the electronic and nuclear degrees of freedom. Pseudopotentials were of the Martins-Troullier type.[40] Amorphous samples were generated by two means: (1) Thermal quench of the liquid from 973K to 300K at different rates. (2) Application of a tensile load at a rate of −0.25 GPa/ps. In both protocols, four-coordinated Ge defects appeared in the glass. These were all tetrahedral as already found in simulations of the related $GeSb_6$ alloy.[22]

The liquid configuration was generated by first melting the initial crystalline GeSb configuration for 10 ps at 973 K. Amorphous glass configurations were then generated by thermal quenching from the last frame of this liquid configuration. Three different quenching rates were used to cool the material. Firstly, a fast quench, in which the temperature was instantly reduced from 973 to 300 K and the trajectory was equilibrated for another 2 ps essentially yielded a frozen-in liquid configuration with little change in structure from the liquid reference state. Secondly, a medium quench with a cooling rate of approximately 70 K/ps was simulated for 9 ps, yielding a more significant rehybridization of both Ge and Sb local configurations. Thirdly, a slow quench with a cooling rate of approximately 40 K/ps was conducted for 16 ps yielding structural changes similar to the medium cooling rate, but with larger drops in conductivity (see Ref.[11]).

For the pressure anneal, the initial crystalline structure was placed under increasing tensile load at the rate of −0.25 GPa/ps, until the material amorphized at approximately −4.0 GPa (the volume of the box was incrementally increased and the resulting tensile load was determined by measuring the resulting stress tensor). Whether or not this seemingly large tensile load was an

over-estimation of the true yield strength of the material is not known at the moment. It seems likely, however, that the material would have yielded earlier if simulation times and the box size had been larger. After the material yielded, it was allowed to equilibrate for a further 4 ps under the large tensile load. Finally, the load was removed (the material was returned to its original volume), and the recompressed PCM was further allowed to equilibrate for another 2 ps. If the material was not given enough time to disorder at the transition tensile load, it recrystallized again when recompressed. This should not impact the metastability of the amorphous state in a real device, as the time scales in a technical application would at least be an order of magnitude larger than those accessed by the simulation, giving the material ample time to fully disorder.

Compressibilities (for the EOS curves) were computed[41] by varying the volume of selected frames from the dynamics trajectories, using an increased cutoff of 60 Ryd. The coordinates of each configuration were relaxed via damped dynamics until the largest atomic force on the atoms was less than 0.001 Ryd/Bohr. Energies were converged to 10^{-6} Ryd, with tighter convergence criteria on a few test systems (10^{-10} Ryd) yielding indistinguishable results. To estimate adiabatic compressibilities, the volume of the glass was changed isotropically from a reference point without relaxing any structural degree of freedom.

Statistical uncertainties for the simulation data were generated by averaging over several separate configurations from the liquid/amorphous trajectories. The uncertainties for the "liquid/solid" data were generated by averaging over 5 initial frames separated by 2 ps from the liquid simulation. The uncertainties for the "glass/solid" amorphous data were generated by averaging over the structures from the last frame from each thermal quenching protocol. Each point in the EOS curves was structurally minimized at the given volume. The pressure and number of 4-coordinated Ge atoms were obtained after convergence of these structural minimizations.

III. THEORY

It is usually possible to interpret the order parameter Φ of a Landau theory microscopically. While Φ generally quantifies the amount of symmetry breaking, it can also relate to densities. For example, the gas-liquid transition can be cast as a Landau theory, although both phases are perfectly isotropic. A transition can only occur, if there is a feedback mechanism, e.g., a spin in the ferromagnetic Ising model tends to align spins on adjacent sites, which then stabilize the original spin. If the feedback is strong compared to thermal fluctuations, symmetry breaking can occur even without external field. It was argued that such a feedback must exist between different Ge atoms with glassy disorder, because otherwise one can explain neither why disordered Ge-Sb alloys "relax away" from the crystal nor why the crystallization pressure p_c increases rapidly with the concentration of Ge or Si dopants in Sb.[12] This observation motivates us to associate the order parameter with the number density of atoms with local order not occurring in the crystal, e.g., that of non-octahedrally coordinated Ge atoms.

Since the amorphous-crystalline transformation is discontinuous, we propose to use the regular expression for the free energy of the lattice gas model

$$F_{\rm gl} = \frac{A}{2}(V_{\rm a} - V)\Phi^2 - \frac{B}{3}\Phi^3 + \frac{C}{4}\Phi^4, \qquad (1)$$

where the three coefficients A, B, C are positive, V is the volume and $V_{\rm a}$ is the volume above which the reference crystal is unstable against amorphization (normalized, for instance, on the unit cell of the reference crystal). We neglect the temperature dependence of all parameters, because our experiments are conducted at room temperature and thermal effects in related stress-induced transformations were found to be weak.[42] We note that the third-order term is symmetry allowed if the order parameter relates to a density (of defects), since the density remains invariant under a symmetry transformation. If, however, the order parameter related to a displacive mode from a crystal with inversion symmetry, then the third-order term would no longer symmetry allowed, because it would change sign under a mirror reflection. Moreover, we cannot replace the term $A(V_{\rm a} - V)\Phi^2/2$ with $A(p - p_{\rm a})\Phi^2/2$, because we want to ascertain the non-analytical behavior of the density near the phase change point.

An alternative free energy expression $F_{\rm dm}$ can be motivated from systems in which displacive modes break inversion symmetry.[43] The simplest dependence of $F_{\rm dm}$ on Φ producing such a discontinuous transition reads

$$F_{\rm dm} = \frac{A'}{2}(V_{\rm a} - V)\Phi^2 - \frac{C'}{4}\Phi^4 + \frac{D'}{6}\Phi^6, \qquad (2)$$

where the coefficients A', C', and D' are again positive. In the specific case, one could argue that the motion of Ge atoms from quasi-octahedral to tetrahedral sites reflect such a displacive mode. Alternatively, collective modes such as they occur in the phase transformation between (resonant-bonding) simple cubic phase of antimony and its (symmetry-broken) α-arsenic structure (A7) would obey Eq. (2). The identification of the correct interpretation necessitates additional information about the microscopic order, which is discussed further below.

The values of Φ minimizing the free energy satisfy $\partial F/\partial\Phi = 0$ in all phases, $\Phi = 0$ in the crystal, and

$$\Phi = \begin{cases} \frac{B}{2C}\left\{1 + \sqrt{1 + \frac{4AC}{B^2}(V - V_{\rm a})}\right\} & F_{\rm gl}\ \text{glass} \\ \sqrt{\frac{C'}{2D'}\left\{1 + \sqrt{1 + \frac{4A'D'}{C'^2}(V - V_{\rm a})}\right\}} & F_{\rm dm}\ \text{glass}, \end{cases} . \qquad (3)$$

as well as $\partial^2 F/\partial\Phi^2 > 0$. When $\partial^2 F/\partial\Phi^2$ approaches 0^+, small thermal fluctuations can induce the phase change.

To introduce coupling to external pressure, we need an expression for the Gibbs free energy of the crystal. For the semi-quantitative analysis pursued here, we restrict ourselves to a scalar theory and thus use the volume V rather than the strain as the second state variable of our material. Because we are interested in the EOS over a large pressure range, an expression that is only quadratic in volume would be too inaccurate. We therefore resort to a Gibbs free energy of the crystal, which includes stiffening with pressure.[44]

$$G_{\rm cr} = \frac{B_0 V}{B_0'}\left\{1 + \frac{(V_0/V)^{B_0'}}{B_0' - 1}\right\} - \frac{B_0 V_0}{B_0' - 1} + pV. \qquad (4)$$

Here V_0 and B_0 denote the specific volume and the bulk modulus at zero pressure, while $B_0' \equiv dB/dp$ is a measure for pressure-induced stiffening. Many simple crystals, take values in between 3.5 and 4, irrespective of the nature of the chemical bonds. This is why we use $B_0' = 3.75$ as a generic value.

Depending on the model used, the total Gibbs free energy per atom reads either $G_{\rm gl} = G_{\rm cr} + F_{\rm gl}$ for the lattice-gas model or $G_{\rm dm} = G_{\rm cr} + F_{\rm dm}$ for the displacive-mode approach. In either case, minimizing G with respect to V results in the following EOS:

$$p(V) = \frac{B_0}{B_0'}\left\{\left[\left(\frac{V_0}{V}\right)^{B_0'} - 1\right]\right\} + \frac{A}{2}\Phi^2, \qquad (5)$$

which reduces to the Murnaghan equation of state[44] for a perfect crystal. To yield the EOS of the glass, we insert the appropriate solutions for $\Phi(V)$ from Eq. (3).

The bulk modulus is defined as $B \equiv -\partial p/\partial \ln V$. The derivative can be taken with two different side constraints. If the system is given enough time to relax to the (potentially metastable) equilibrium, i.e., assuming $\partial G/\partial\Phi = 0$, we obtain the isothermal bulk modulus B_T. Alternatively, when compression is too fast to allow structural relaxation within the bulk, i.e., for $\Phi = \text{const}$, the adiabatic bulk modulus B_S is obtained. Since the ideal-gas contribution to elasticity is negligibly small for solids, we disregard it in the calculation of B_T and B_S.

IV. RESULTS

A. Equation of State

We determined the EOS for two different Ge_xSb_{1-x} compositions and adjusted the free parameters of the Gibbs free energy to match the data. Results are shown for $x = 0.15$ in Fig. 5 and for $x = 0.25$ in Fig. 6. B_0, V_0, and one parameter in $F(\Phi)$ can be used to gauge the units of p, V, and Φ. For the latter we chose $C = B_0V_0$ and $D' = B_0V_0$ in case of the gas-liquid and displacive mode picture, respectively. $B_0' = 3.75$ is a quasi-universal value, which leaves us with three free dimensionless adjustable parameters, i.e., $V_{\rm a}/V_0$, and either A/C, B/C or A'/D', B'/D'. The three adjustable dimensionless parameters can be gauged to match exactly three observables. We chose them to be $p_{\rm c}$, the latent density at the crystallization transition, and the glass density at ambient pressure. Latent density and $p_{\rm c}$ could be determined with relatively high accuracy, because amorphous and crystalline spectra coexisted at $p_{\rm c}$. Once the dimensionless parameters are fixed, we have no more possibility to "fudge" the curves.

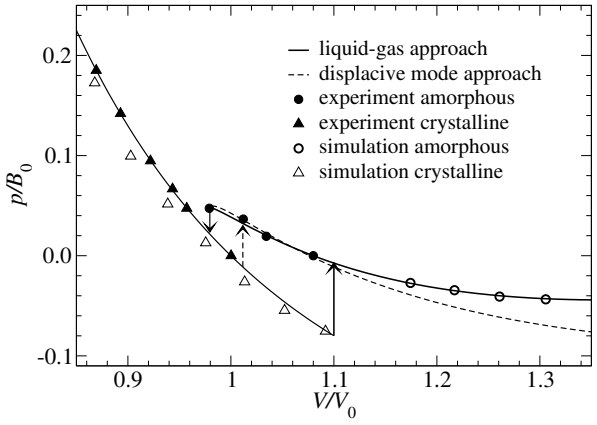

FIG. 5: The equation of state of $Ge_{0.15}Sb_{0.85}$ as measured experimentally (closed symbols) and determined numerically (open symbols). Full (black) and dotted (grey) lines represent the lattice-gas and displacive-mode Landau approach, respectively. Arrows indicate the instability points. V_0 and B_0 represent experimental volume per unit cell and bulk modulus at ambient conditions, respectively.

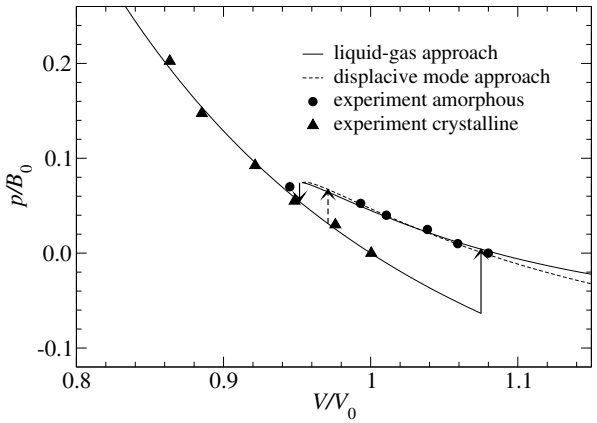

FIG. 6: The equation of state of $Ge_{0.25}Sb_{0.75}$. Symbols as in Figure 5.

In Fig. 5 we find almost perfect agreement for the $x = 0.15$ alloy when calculations are based on the Gibbs free energy of the liquid-gas model. We interpret the almost perfect agreement for the $x = 0.15$ curve between Landau theory and simulation as a fortuitous cancellation of two small errors: As mentioned above, we estimated the isothermal EOS for the glass with high-temperature simulations. This leads to an overestima-

tion of the density of $\lesssim 1\%$. At the same time, our DFT simulations underestimate density by $\lesssim 1\%$, as can be seen from the crystalline reference data. The displacive mode picture is less satisfactory, except for the crystalline phase, where both models coincide. Particularly the small hysteresis is flawed, because it indicates that the (dm) glass has smaller enthalpy than the crystal at ambient conditions. Similar trends are observed for the $x = 0.25$ alloy as shown in Fig. 6. The parameters used to produce the Landau theory are summarized in Table I.

$\mathbf{Ge_{0.15}Sb_{0.85}}$			$\mathbf{Ge_{0.25}Sb_{0.75}}$		
a	b	v_a	a	b	v_a
24.88	24.19	1.10	20.89	20.38	1.08
a'	b'	v'_a	a'	b'	v'_a
18.93	10.73	1.01	16.52	6.99	0.97

TABLE I: (Color online.) Summary of the dimensionless parameters used for the fitting of the EOS of $\mathrm{Ge}_x\mathrm{Sb}_{1-x}$. The variables a, b, v_a refer to the lattice gas model, while a', b', v'_a relate to the displacive-model picture.

Two more results support the lattice-gas ansatz: First, the termination point of the crystalline EOS, as determined from experimental data, coincides with a theoretical prediction[11] of the (negative) amorphization pressure of $p = -4$ GPa. For $x = 0.25$, the predicted instability point of the displacive mode model lies within the experimentally observed stability regime, while the lattice-gas model correctly predicts the material to remain stable at non-negative pressures. Second, we find that the EOS of the *quenched* glass (isotropic compression of the DFT glass not allowing structural relaxations) are almost identical with those of the crystal, except that they are shifted by 3 GPa (not shown explicitly). This last value coincides with the numerical value we obtain for the term $-A\Phi^2/2$ in Eq. (5) for the gl-Landau approach. As a consequence, we find almost identical values for $B_S^{\mathrm{DFT}} - B_T^{\mathrm{DFT}} = 14.7$ GPa and $B_S^{\mathrm{gl}} - B_T^{\mathrm{gl}} = 15.1$ GPa while the dm result $B_S^{\mathrm{dm}} - B_T^{\mathrm{dm}} = 10.6$ GPa is less good.

B. Reversibility

The Landau approach is based on the idea that structural changes are reversible. As it is currently not feasible to attain negative pressures in DACs, we cannot produce direct experimental evidence that the full transition from the glass to the crystal can be reversed through tensile loads. However, as demonstrated in Fig. 7, we reversed most of the partial crystallinity, when decompressing from a pressure just a little below p_c. Only when crystallinity exceeded 25% did we no longer recuperate the amorphous phase after decompression. Partial crystallinity can be rationalized theoretically by considering the small, but experimentally unavoidable pressure anisotropies in the DAC. Its quantitative modeling would require the use of (direction-dependent) square-gradient corrections to the enthalpy, which is beyond the scope of this work.

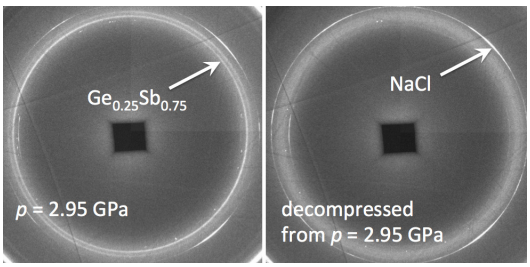

FIG. 7: XRD spectra of amorphous $\mathrm{Ge}_{0.25}\mathrm{Sb}_{0.75}$ compressed to $p = 2.95$ GPa (left) and decompressed back to ambient pressure (right). The partial crystallinity is reversed. The Bragg peaks are related to the NaCl reference crystal included in the DAC. Peak intensities are shown in Fig. 8.

The compression-decompression cycle, from which the snapshots in Fig. 7 are deduced, is presented in more detail in Fig. 8. The maximum pressure was chosen to be just at the onset of crystallization. At that point, two phases can coexist due to small pressure heterogeneities in the DAC chamber. After decompression back to ambient pressures, the crystallinity decreases to some few percents and remains below 1%. A small densification of $O(1\%)$ remains of the initially sputtered sample after decompression from 3.0 GPa.

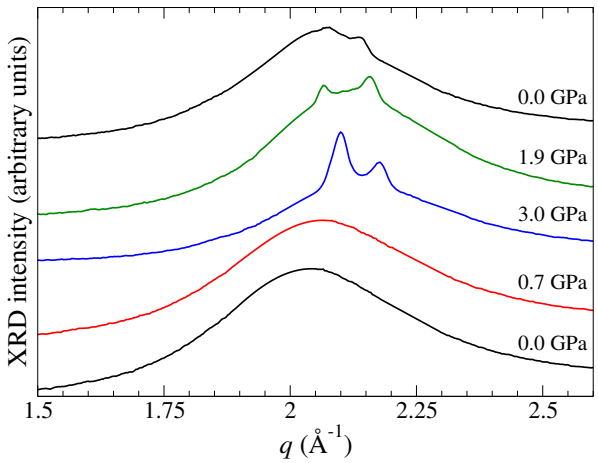

FIG. 8: (Color online.) Compression decompression cycle of $\mathrm{Ge}_{0.25}\mathrm{Sb}_{0.75}$. The partial crystallinity attained at $p = 3.0$ GPa is essentially lost.

C. Microscopic interpretation of the order parameter

The microscopic interpretation of the order parameter still needs to be substantiated. To this end we exploit the observation by Mazzarello *et al.*[20], who identified weak features in Raman spectra for frequencies $190\mathrm{cm}^{-1} <$

$\omega < 250\text{cm}^{-1}$. They could be related to modes involving tetrahedrally-coordinated germanium atoms. We were able to fit the Raman data with 3(4) peaks in the amorphous (crystalline) phase of $Ge_{0.15}Sb_{0.85}$. Assuming that the intensity of each peak is proportional to the density of the corresponding atoms, it is possible to deduce the order parameter from Raman experiments as the ratio of the peak intensities related to the vibrations of tetrahedrally and six-coordinated Ge atoms.

Fig. 9 demonstrates consistency of the number of tetrahedral Ge atoms as deduced from the lattice-gas based Landau theory, the Raman experiments, and the simulations. As can be deduced from the scan indices in Fig. 9, the number of tetrahedral Ge atoms recuperates after decompression in the amorphous phase, e.g., after scan 6, but no more at $p > 0$ after crystallization, e.g., after scan 8. Note also that the Landau theory predicts the glass to become unstable at a similar negative pressure where simulations no longer find octahedral Ge atoms (acting as "predetermined breaking points"). Simulation providing the order parameter are discussed in the remainder of this section.

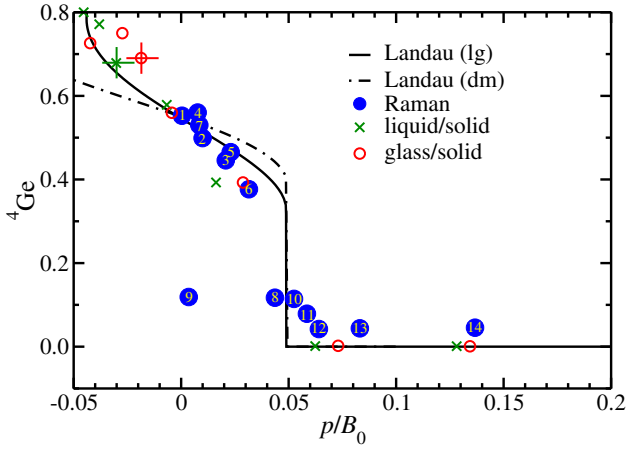

FIG. 9: (Color online.) Relative number of tetrahedrally-coordinated Ge atoms in $Ge_{0.15}Sb_{0.85}$ obtained after constant-volume energy minimizations of the $T = 973$ K liquid (green crosses) and the $T = 300$ K glass (red circles). For clarity, representative error bars are given for one data point only. Full lines reflect Landau theory. Landau theory and Raman data (blue circles) have been normalized to match simulations results near zero pressure. Numbers on the Raman symbols index the scans.

Fig. 10 compares the liquid structure of $Ge_{15}Sb_{0.85}$ at 973 K with that resulting from the slow temperature quench at 300 K. Both structures are highly disordered, as can be seen in Figs. 10a–b. However, there are subtle and nevertheless important differences in the two structures. This is made evident in Fig. 10c, which shows the coordination probabilities of both Ge and Sb measured in the simulation leading to the shown structures. In the liquid, germanium is approximately 50% 4-coordinated and only 40% 3-coordinated. Once cooled, the number of 4-coordinated germanium increases to approximately 70%,

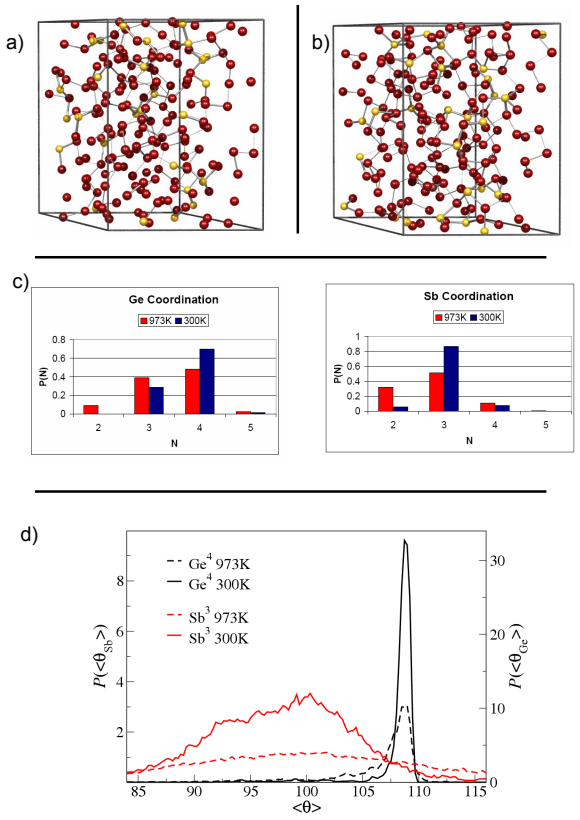

FIG. 10: (Color online) Comparison between local structures for liquid $Ge_{0.15}Sb_{0.85}$ at (a) 973K and (b) the quenched amorphous samples at 300K. (c) Coordination probability for Ge and Sb in each of the simulations. (d) Average-angle distributions around 4-coordinated Ge and 3-coordinated Sb. The majority of 4-coordinated Ge atoms are in tetrahedral configurations, with bond angle distributions centered around 109°.

with the remainder being 3-coordinated. This increase in tetrahedral germanium coordination can also be seen from the average-angle distribution functions shown in Fig. 10d. These distributions measure the average-angle around a given atom-type with a particular coordination. The distributions show that the signal of tetrahedrally bonded germaniums (there are sharp peaks centered at 109°) increases by a factor of 3 after the quenching protocol. There is also a change in the antimony average structure, although not as pronounced as in the germanium case. After the thermal quench, 86% of the antimony end up in their preferred 3-coordinated state, as can be seen in Fig. 10c.

V. CONCLUSIONS

The pressure anneal shows a similar propensity to generate tetrahedral germanium as the temperature anneal. This can be seen in the comparison between the struc-

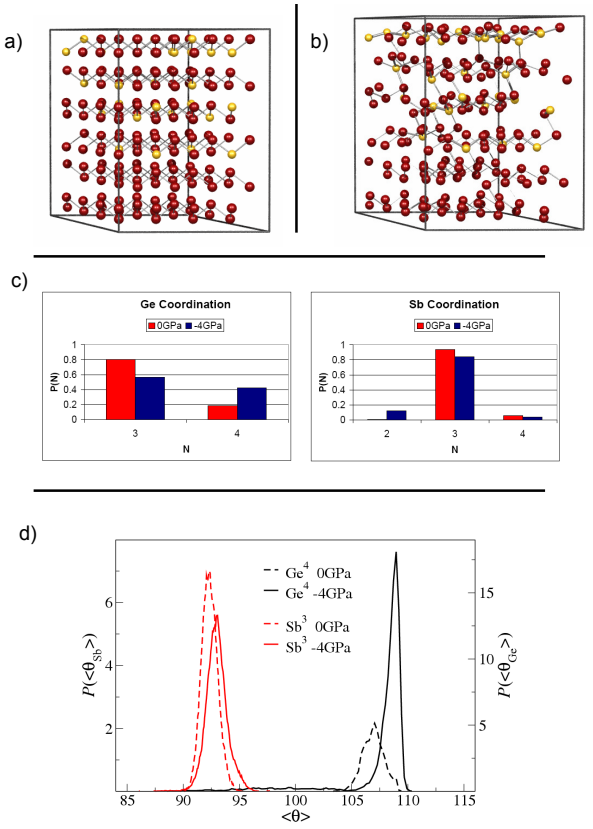

FIG. 11: (Color online) Comparison between local structures for (a) crystalline $Ge_{0.15}Sb_{0.85}$ and (b) a pressure annealed "amorphous" samples at 300K. (c) Coordination probability for Ge and Sb in each of the simulations. (d) Average-angle distributions around 4-coordinated Ge and 3-coordinated Sb. The majority of 4-coordinated Ge atoms are in tetrahedral configurations, with bond angle distributions centered around 109°.

ture of a 4 ps equilibrated crystal (0 GPa) and that of system equilibrated for 4 ps at −4.0 GPa (tensile) load in Fig. 11. While the lamellar ("long-range") structure of the A7 parent antimony lattice remains visible in the streched sample, the local environment of many germanium atoms have changed. Specifically, in the A7 crystal structure each atom has three short bonds to neighbors within their lamella and three long bonds to next-nearest neighbors located in the adjoining layer. Under sufficiently large tensile load, a few of the germaniums break one of their short bonds and create a tetrahedral complex by forming two short bonds with the adjoining layer. This process is akin of the so-called "umbrella" flip[15] in the 225 material. In the current situation, it can be seen as a self-healing process, in which the onset of delamination is impeded by germanium atoms adjoining two departing lamella back together. This structural rearrangement is quantified in the coordination data presented in Fig. 11c. In the crystal, only 20% of the germaniums are 4-coordinated. This number doubles in the annealed configuration and is expeted to grow further if the system were given more time to relax. The tetrahedral rehybridization is also evident in the average angular distribution function in Fig. 11d, with a clear increase in the number of 4-coordinated tetrahedral Ge (average bond angle around the element about 109°).

In summary, we propose that the amorphous phase of optoelectronic PCMs should not be regarded as regular glasses produced by quenching a fluid. Instead, amorphization in these systems can be interpreted as a condensation of defects with characteristic local order. A Landau theory with three dimensionless parameters, which is based on this picture, not only produces a highly accurate equation of state for the glass, it also predicts similar results as DFT-based simulations for the amorphization stress and the difference between adiabatic and isothermal bulk modulus. Moreover, the integrated Raman signal related to tetrahedrally coordinated germanium atoms (which are not present in the crystal) correlates with the order parameter. We also provide direct experimental evidence that stress-induced partial crystallinity is indeed reversible when stress is released.

The presented results support the idea that differences in the (mechanical) properties between our amorphous and disordered PCMs stem predominantly from changes in the *local* structure, even if the detailed intermediate- or long-range structure certainly affect response function as well. However, as already found previously[14], ordering of species onto sublattices in the crystal is not necessary to explain the strong contrast between amorphous and crystalline PCMs. Local (athermal) dynamics suffice to invoke the phase change by stress, which explains why PCMs can be switched so rapidly.

Acknowledgments

We thank the Nanofab Lab at the Univeristy of Western Ontario for assistance during sample preparation and the ANKA synchrotron light source of FZ Karlsruhe for provision of beam time at the PDIFF beamline. We also acknowledge computer time on IBM Watson's Blue Gene/L and FZ Jülich's Blue Gene/P supercomputers as well as support from the German Research Science foundation (DFG) through grant Mu 1694/6-1.

* Email: martin.mueser@mx.uni-saarland.de

[1] S. R. Ovshinsky, Phys. Rev. Lett. **21**, 1450 (1968).

[2] N. Yamada, E. Ohno, K. Nishiuchi, N. Akahira, and M. Takao2, J. Appl. Phys. **69**, 2849 (1991).

[3] A. L. Lacaita, Solid-State Electron. **50**, 24 (2006).
[4] D. Lencer, M. Salinga, B. Grabowski, T. Hickel, J. Neugebauer, and M. Wuttig, Nature Mater. **7**, 972 (2008).
[5] D. Newns, B. Elmegreen, X. H. Liu, and G. Martyna, J. Appl. Phys. **111**, 084509 (2012).
[6] A. V. Kolobov, J. . Haines, A. Pradel, M. . Ribes, P. . Fons, J. Tominaga, Y. Katayama, T. . Hammouda, and T. Uruga, Phys. Rev. Lett. **97**, 035701 (2006).
[7] M. Krbal, A. V. Kolobov, J. Haines, P. Fons, C. Levelut, R. Le Parc, M. Hanfland, J. Tominaga, A. Pradel, and M. Ribes, Phys. Rev. Lett. **103**, 115502 (2009).
[8] S. Caravati, M. Bernasconi, T. D. Kühne, M. Krack, and M. Parrinello, Phys. Rev. Lett. **102**, 205502 (2009).
[9] M. Xu, Y. Meng, Y. Q. Cheng, H. W. Sheng, and X. D. H. andE. Ma, J. Appl. Phys. **108**, 083519 (2010).
[10] Z. Sun, J. Zhou, Y. Pan, Z. Song, H.-K. Mao, and R. Ahuja, Proc. Natl. Acad. Sci. **108**, 10410 (2011).
[11] D. Shakhvorostov, R. A. Nistor, L. Krusin-Elbaum, G. J. Martyna, D. M. Newns, B. G. Elmegreen, X. Liu, Z. E. Hughes, S. Paul, C. C. Jr., et al., Proc. Natl. Acad. Sci. **106**, 10907 (2009).
[12] D. Shakhvorostov and M. H. Müser, EPL **93**, 36002 (2011).
[13] S. Raoux, D. Ielmini, M. Wuttig, and I. Karpov, MRS Bullet. **37**, 118 (2012).
[14] J. Kalikka, J. Akola, J. Larrucea, and R. O. Jones, Phys. Rev. B **86**, 144113 (2012).
[15] A. V. Kolobov, P. Fons, A. I. Frenkel, A. L. Ankudinov, J. Tominaga, and T. Uruga, Nature Mater. **3**, 703 (2004).
[16] K. S. Andrikopoulos, S. N. Yannopoulos, G. A. Voyiatzis, A. V. Kolobov, M. Ribes, and J. Tominaga, J. Phys.: Condens. Matter **18**, 965 (2006).
[17] S. Caravati, M. Bernasconi, T. D. Kühne, M. Krack, and M. Parrinello, Appl. Phys. Lett. **91**, 171906 (2007).
[18] J. Akola and R. O. Jones, Phys. Rev. B **76**, 235201 (2007).
[19] J. Akola and R. O. Jones, J. Phys.: Condens. Matter **20**, 465103 (2008).
[20] R. Mazzarello, S. Caravati, S. Angioletti-Uberti, M. Bernasconi, and M. Parrinello, Phys. Rev. Lett. **104**, 085503 (2010).
[21] S. J. Park, M. H. Jang, S.-J. Park, M.-H. Cho, J. K. Kim, D.-H. Ko, and H. C. Sohnb, J. Electrochem. Soc. **157**, H1078 (2010).
[22] M. Micoulaut, J.-Y. Raty, C. Otjacques, and C. Bichara, Phys. Rev. B **81**, 174206 (2010).
[23] M. H. Müser, Eur. Phys. J. B **74**, 291 (2010).
[24] D. Krebs, Ph.D. thesis, RWTH Aachen (2010).
[25] H. K. Mao, P. M. Bell, J. W. Shaner, and D. J. Steinberg, J. Appl. Phys. **49**, 3276 (1978).
[26] J. R. Ferraro, K. Nakamoto, and C. W. Brown, *Introductory Raman Spectroscopy* (Amsterdam:Academic Press, 2003).
[27] T. Naes et al., *A user-friendly guide to Multivariate Calibration and Classification* (UK: NIR Publications, Charlton, Chichester, West Sussex, 2004).
[28] Stellman et al., Science and engineering of composite materials **7**, 1 (1998).
[29] P. Geladi et al., Spectrochimica Acta Part B: Atomic Spectroscopy **59**, 1347 (2004).
[30] O. Y. Rodionova et al., Analytica Chimica Acta **549**, 151 (2005).
[31] B. Vaezian, C. R. Anderton, and M. L. Kraft, Analytical Chemistry Anal. Chem. **82**, 10006 (2010).
[32] H. Lin et al., Applied Spectroscopy **66**, 272 (2012).
[33] T. Alexandrov, BMC Bioinformatics C7-S11 **13**, 1 (2012).
[34] M. Diem et al., Spectroscopy: An International Journal **27** (2012).
[35] R. A. Nistor, Ph.D. thesis, University of Western Ontario (2009).
[36] R. Car and M. Parrinello, Phys. Rev. Lett. **55**, 2471 (1985).
[37] A. D. Becke, Phys. Rev. A **38**, 3098 (1988).
[38] C. Lee, W. Yang, and R. G. Parr, Phys. Rev. B **37**, 785 (1988).
[39] G. J. Martyna, M. L. Klein, and M. Tuckerman, J. Chem. Phys. **97**, 2635 (1992).
[40] N. Troullier and J. L. Martins, Phys. Rev. B **43**, 1993 (1991).
[41] P. Giannozzi, S. Baroni, N. Bonini, M. Calandra, R. Car, C. Cavazzoni, D. Ceresoli, G. L. Chiarotti, M. Cococcioni, I. Dabo, et al., J. Phys. Cond. Matt. **21**, 395502 (2009).
[42] M. Krbal, A. V. Kolobov, J. Haines, A. Pradel, M. Ribes, P. Fons, J. Tominaga, C. Levelut, R. L. Parc, and M. Hanfland, Appl. Phys. Lett. **93**, 031918 (2008).
[43] M. T. Dove, A. P. Giddy, and V. Heine, Ferroelectrics **136**, 33 (1992).
[44] F. D. Murnaghan, Proc. Natl. Acad. Sci. **30**, 244 (1944).